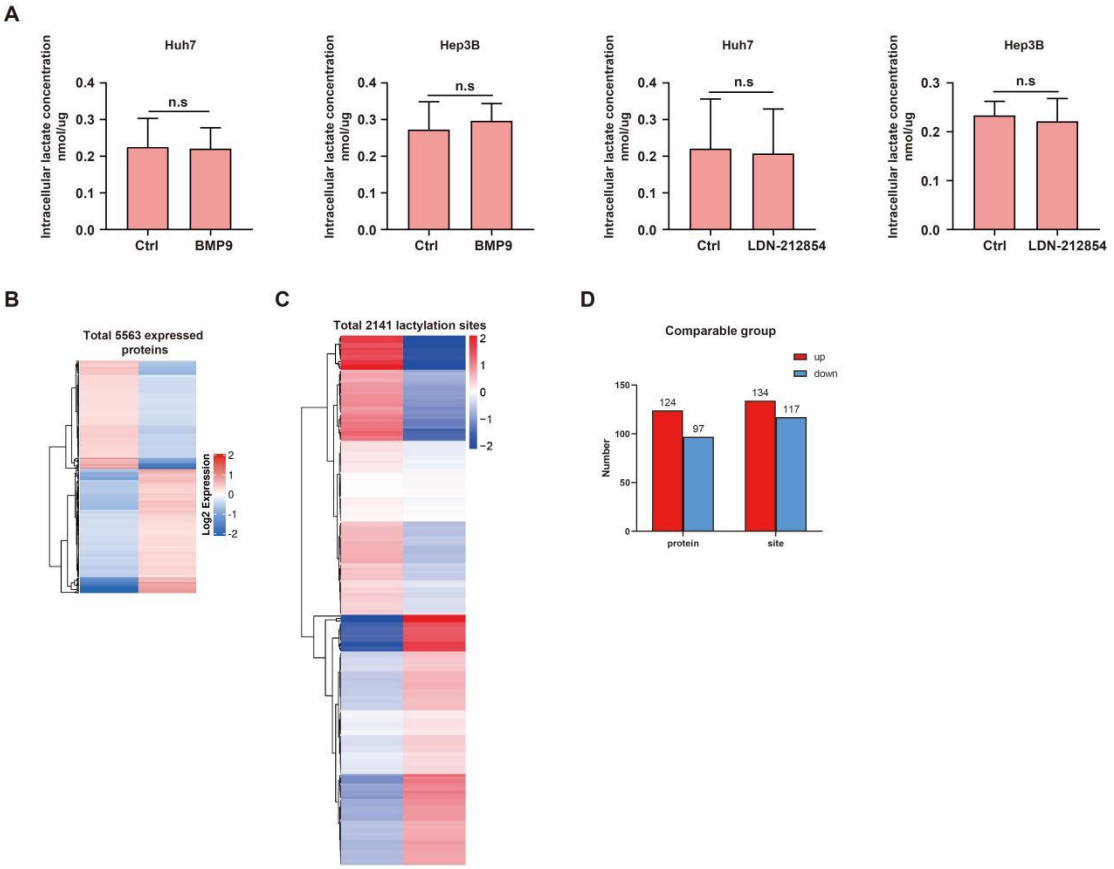

Figure S1. Effects of BMP signaling on intracellular lactate levels and proteomic/lactylomic profiling of LDN-212854-treated HCC cells

A) Measurement of intracellular lactate concentration (nmol/μg protein) in Huh7 and Hep3B cells treated with BMP9 (left two panels) or LDN-212854 (right two panels), compared with their respective controls (Ctrl). Neither BMP9 nor LDN-212854 treatment significantly altered intracellular lactate levels in HCC cells. Data are presented as mean ± SD from three independent biological replicates. p-values were calculated using Student's t-test; n.s., not significant. B) Heatmap showing the expression profile of a total of 5,563 proteins identified by quantitative proteomic analysis in Hep3B cells treated with LDN-212854 versus control. Color scale represents Log2-transformed expression values, with red indicating up-regulation and blue indicating down-regulation. C) Heatmap displaying the abundance profile of a total of 2,141 lactylation sites detected by lactylomic analysis in Hep3B cells treated with LDN-212854 versus control. Color scale represents the relative lactylation level, with red indicating increased and blue indicating decreased lactylation abundance. D) Bar graph summarizing the number of differentially expressed proteins and differentially lactylated sites in Hep3B cells following LDN-212854 treatment. Among the proteins analyzed, 124 were significantly up-regulated and 97 were significantly down-regulated; among the lactylation sites, 134 showed increased abundance while 117 showed decreased abundance. Red bars represent up-regulated entries; blue bars represent down-regulated entries.

A

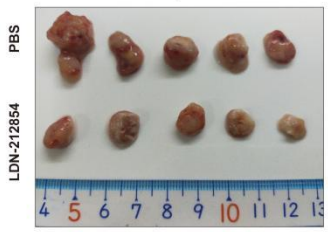

B

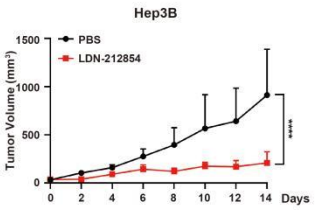

C

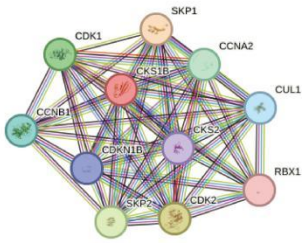

D

Your Input:

		Neighborhood	Gene Fusion	Cooccurrence	Coexpression	Experiments	Databases	Textmining	Homology	Score
CKS1B	Cyclin-dependent kinases regulatory subunit 1; Binds to the catalytic subunit of the cyclin dependent kinases and is essential for their biological function. (79 aa)									

Predicted Functional Partners:

SKP1	S-phase kinase-associated protein 1; Essential component of the SCF (SKP1-CUL1-F-box protein) ubiquitin ligase complex, whi...					●	●	●		0.999
CDK2	Cyclin-dependent kinase 2; Serine/threonine-protein kinase involved in the control of the cell cycle; essential for meiosis, but di...					●	●	●		0.999
SKP2	S-phase kinase-associated protein 2; Substrate recognition component of a SCF (SKP1-CUL1-F-box protein) E3 ubiquitin-protei...					●	●	●		0.999
CDK1	Cyclin-dependent kinase 1; Plays a key role in the control of the eukaryotic cell cycle by modulating the centrosome cycle as w...					●	●		●	0.999
CCNA2	Cyclin-A2; Cyclin which controls both the G1/S and the G2/M transition phases of the cell cycle. Functions through the formati...					●	●	●	●	0.999
CCNB1	G2/mitotic-specific cyclin-B1; Essential for the control of the cell cycle at the G2/M (mitosis) transition; Belongs to the cyclin f...					●	●		●	0.998
CUL1	Cullin-1; Core component of multiple cullin-RING-based SCF (SKP1-CUL1- F-box protein) E3 ubiquitin-protein ligase complexes,...						●	●	●	0.998
CDKN1B	Cyclin-dependent kinase inhibitor 1B; Important regulator of cell cycle progression. Inhibits the kinase activity of CDK2 bound t...						●	●	●	0.997
CKS2	Cyclin-dependent kinases regulatory subunit 2; Binds to the catalytic subunit of the cyclin dependent kinases and is essential f...					●	●	●	●	0.993
RBX1	E3 ubiquitin-protein ligase RBX1, N-terminally processed; E3 ubiquitin ligase component of multiple cullin-RING-based E3 ubiq...						●	●	●	0.988

E

Interactor	Experiments	Homologs	Category	Interaction Score	Confidence
CDK2 Cyclin-dependent kinase 2	17	20	Small-scale	0.986	High
CDK1 Cyclin-dependent kinase 1	13	20	Small-scale	0.983	High
CDK3 Cyclin-dependent kinase 3	7	20	Small-scale	0.962	High
PMYT1 Membrane-associated tyrosine- and threonine-specific cdc2-inhibitory kinase	3	7	High-throughput	0.861	High
CKS2 Cyclin-dependent kinases regulatory subunit 2	2	5	High-throughput	0.789	High

Figure S2. LDN-212854 suppresses Hep3B-derived xenograft tumor growth, and identification of CKS1B-interacting proteins through database analysis.

A) Representative gross images of subcutaneous xenograft tumors harvested from NCG mice bearing Hep3B-derived tumors treated with PBS (top row) or LDN-212854 (bottom row, 6 mg/kg, intraperitoneal injection, twice daily for 10–14 days). The ruler (cm) is shown for scale reference. LDN-212854 treatment markedly reduced tumor size compared with the PBS control group (n = 5 per group). B) Tumor growth curves of Hep3B-derived xenograft tumors in mice treated with PBS (black) or LDN-212854 (red). Tumor volumes (mm^3) were measured every two days over a 14-day treatment period. LDN-212854 significantly inhibited tumor growth compared with the PBS control. Data are presented as mean ± SD (n = 5 per group). p-values were calculated using Student's t-test; ****$p < 0.0001$. C) Protein–protein interaction (PPI) network of CKS1B and its top predicted functional partners, generated using the STRING database (https://string-db.org/). Nodes represent proteins, and edges represent predicted functional associations, with edge thickness indicating the confidence score of the interaction. CKS1B exhibits strong interactions with multiple cell cycle- and ubiquitin ligase-related proteins, including CDK1, CDK2, CDK3, CCNA2, SKP1, SKP2, CUL1, RBX1, and CDKN1B (p27). D) Tabulated list of CKS1B's top predicted functional partners retrieved from the STRING database, including SKP1, CDK2, SKP2, CDK1, CCNA2, CUL1, CDKN1B, CKS2, and RBX1. The table provides functional annotations and the corresponding evidence channels (Neighborhood, Gene Fusion, Co-occurrence, Co-expression, Experiments, Databases, Text-mining, and Homology), along with the combined

confidence Score for each interaction. All listed partners exhibit high confidence scores (≥0.988). E) Tabulated list of CKS1B-interacting proteins retrieved from the HitPredict database (https://www.hitpredict.org/), including CDK2, CDK1, CDK3, PMYT1, and CKS2. The table summarizes the number of supporting Experiments and Homologs, the experimental Category (Small-scale or High-throughput), the Interaction Score, and the Confidence level for each interactor. CDK1, CDK2, and CDK3 are identified as high-confidence CKS1B interactors with strong experimental support, providing the rationale for their selection as downstream effectors in subsequent functional studies.

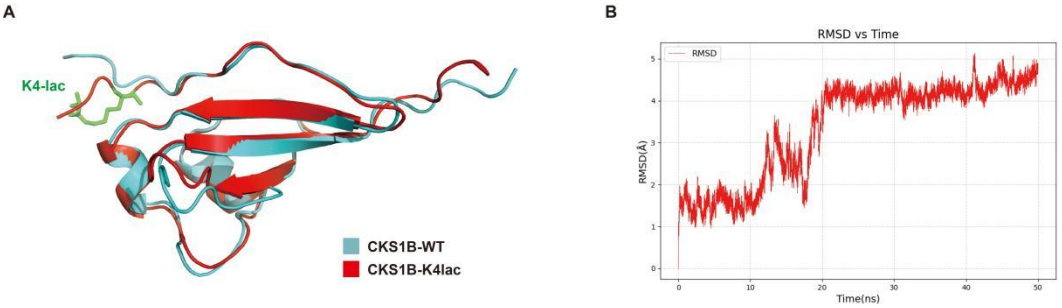

Figure S3. Molecular dynamics simulation reveals K4 lactylation-induced conformational changes in CKS1B.

A) Structural superposition of wild-type CKS1B (CKS1B-WT, cyan) and K4-lactylated CKS1B (CKS1B-K4lac, red) following 50 ns of molecular dynamics (MD) simulation. The lactyl group attached to lysine 4 (K4-lac) is highlighted in green stick representation. Compared with CKS1B-WT, CKS1B-K4lac displays noticeable conformational rearrangements, particularly within the central β-sheet region and the surrounding loop domains, indicating that K4 lactylation induces local structural perturbations in CKS1B. B) Root-mean-square deviation (RMSD) trajectory of CKS1B-K4lac relative to its initial structure over a 50 ns MD simulation. The RMSD value (Å) gradually increased from approximately 1.5 Å during the first 10 ns to a plateau of approximately 4.5–5.0 Å after 20 ns, suggesting that K4 lactylation drives CKS1B toward a new, stable conformational state distinct from its unmodified form. The stepwise increase in RMSD reflects a progressive structural transition rather than random fluctuation, supporting the notion that K4 lactylation exerts a defined conformational effect on CKS1B.

CACTTACACCCCTGCCACCTCCTCCAGTACCAATTTACCCATGGCCAAACACAGGGTGATGTGTAGGAACCTGAAAGCACGTCTCCGACCTCAGCTGCAAAACTGTGG
AGTCCCACACACTAGACTTTATATTCCAGCATTTCCTCTCACCATTACATTTTTGCTTTTTTCCATCCTTACATTACCTTTACCACATTTTTGTTTTTCCCATAATTACATTAGA
TAAGGCAATGGCTAGACGTGGTCTTTTACTAACTTGTTCTATTGGGAGCGGACGAGAAAAAAAAAAAAAGACAAACCCTAGAAATGTCTTCAGGTCCCAGCCATGTTT
AGGAAAATACTTGAAGGCTTCTGCGGTGAGAGTGCTACCTGGTAAGGGCGTATGGACACACGTGGAGGGCAAGAAATGAATTTGGGTCTGGTGCCGAAACATCTTT
CCACTGCTGTGATTTTGTTTTCTGGTCAGAGTAATAATGCTCGTTGTAAAATAAATAAATAAATAATACATAAAAAGGAAAAGGAAAATTCAGAGAAAATGAAAACAA
CTCGTAATCAACGTGCTTTTTGGATGTGAACTGCTCCCTTTGGGAGGGCAATGGAGAAGTGAGGACGCACTGGGTATCTGGCCCGGAACAGCCGGCAGTGGGTACA
CCCTGCCTGGTGAATTCGACCGGGGTTTTGGGGGACCCGCCACCCAAGGGCCGAAGAGCAGGGCCGCCCTACGGGCGCTCCCATTTGGCCACCTGAGTGGCGACTT
GGCGCCTTCCTCGGAGCAGCTCCGGGGTTCCGTCGTCCCGGTTCCCACTGGTCCCTTACGCAGAGACCAAAGGCAGGAACCTTCCCTCGTAACTATCCACCGACTGAA
AATAGATTCTGAGTCCGCCCCCGCCCCTCCCCCCTTAAAATCCTCCCCACTCTTAAAATCCTCCCCTTTAAAGGGAGCCACAGGGTGACGCCGGGGGAGTTTGCGGAA
GCGCTAACCGCGTTGGGGCCTAGGGCGGATCCCGTGATTGGGACAGGCCCCGCCCCCGGCTCCACTTCCCCCATTGTGTGAGCGGCTCGGGCCTAGGCCCCGCCCCCC
TCCGGAGGCCCGGCCACTCCCCTTTTCCACCC

CCCCTTGGCTCATTTCCGGCCGCCGCCGCTACCGCTAGCCTGTAAGGAGGATTCGGCAGAGGGAAGAAACAACAGCCGCCATCTTGTTTGTGTGCTAGGCTGGGGGG
GAGAGAGGGCGAGAGAGAGCGGGCGAGAGTGGGCAAGCAGGACGCCGGGCTGAGTGCTAACTGCGGGAGCCAGAGAGTGCGGAGGGGAGTCGGGTCGGAGA
GAGGCGGCAGGGGCCGAGACAGTGGCAGGGGGCCCGGGGCGCACGGGCTGAGGCGACCCCCAGCCCCCTCCCGTCCGCACACACCCCCACCGCGGTCCAGCAGC
CGGGCCGGCGTCGACGCCTAGGGGGGACCATTACATAACCCCGCGCCCCGCGGCGTCTTCTCCCGCCGCCGCGGGCGGCCCCGAACGGAGCCCCGGGGGGCGGGC
GCTCCCAGCACCTGGCCGCCGGCGGTGGGGGCCGTAGCAGCGGCCGTATTTATTTATTTTCCGCGGGAAAGGAAGGCGAAGGAGGGGAGCGCGGCGCGAGGAGG
GGCCGCCTGCGCCGCCGCCGGAGCGGGGCCTCCTCGGTGGGCTCCGCGTCGGCGCGGGCGTGCGGGCGGCGCTGCTCGGCCCGGCCCCCTCGGCCCTCTGGTCCGG
CCAGCTCCGCTCCCGGCGTCCTTGCCGCGCCTCCGCCGGCCGCCGCGCGATGTGAGGCGGCGGCGCCAGCCTGGCTCTCGGCTCGGGCGAGTTCTCTGCGGCCATTA
GGGGCCGGTGCGGCGGCGGCGGCGCGCGGAGCGCGGCGGCAGGAGGAGGGTTCGGAGGGTGGGGGCGCAGGCCCGGGAGGGGGCACCGGGAGGAGGTGAGTGT
CTCTTGTCGCCTCCTCCTCTCCCCCCTTTTCGCCCCCGCCTCCTTGTGGCGATGAGAAGGAGGAGGACAGCGCCGAGGAGGAAGAGGTTGATGGCGGCGGCGGAGCT
CCGAGAGACCTCGGCTGGGCAGGGGCCGGCCGTGGCGGGCCGGGGAC

Figure S4. Identification of GC-SBE motifs within the p300 promoter region.

Nucleotide sequence of the human p300 (EP300) gene promoter region (~2 kb upstream of the transcription start site), in which a total of eight putative GC-rich SMAD-binding element (GC-SBE) motifs were identified through in silico sequence analysis.